

Faithful Effective-One-Body waveforms of small-mass-ratio coalescing black-hole binaries

Thibault Damour¹ and Alessandro Nagar²

¹*Institut des Hautes Etudes Scientifiques, 35 route de Chartres, 91440 Bures-sur-Yvette, France*

²*Dipartimento di Fisica, Politecnico di Torino, Corso Duca degli Abruzzi 24, 10129 Torino, Italy and INFN, sez. di Torino, Via P. Giuria 1, Torino, Italy*

(Dated: October 27, 2018)

We address the problem of constructing high-accuracy, faithful analytic waveforms describing the gravitational wave signal emitted by inspiralling and coalescing binary black holes. We work within the Effective-One-Body (EOB) framework and propose a methodology for improving the current (waveform) implementations of this framework based on understanding, element by element, the physics behind each feature of the waveform, and on systematically comparing various EOB-based waveforms with “exact” waveforms obtained by numerical relativity approaches. The present paper focuses on small-mass-ratio non-spinning binary systems, which can be conveniently studied by Regge-Wheeler-Zerilli-type methods. Our results include: (i) a resummed, 3PN-accurate description of the inspiral waveform, (ii) a better description of radiation reaction during the plunge, (iii) a refined analytic expression for the plunge waveform, (iv) an improved treatment of the matching between the plunge and ring-down waveforms. This improved implementation of the EOB approach allows us to construct complete analytic waveforms which exhibit a remarkable agreement with the “exact” ones in modulus, frequency and phase. In particular, the analytic and numerical waveforms stay in phase, during the whole process, within $\pm 1.1\%$ of a cycle. We expect that the extension of our methodology to the comparable-mass case will be able to generate comparably accurate analytic waveforms of direct use for the ground-based network of interferometric detectors of gravitational waves.

PACS numbers: 04.25.Nx, 04.30.-w, 04.30.Db

I. INTRODUCTION

Coalescing black hole binaries are among the most promising gravitational wave (GW) sources for the currently operating ground-based detectors like GEO/LIGO/VIRGO. The most useful part of the waveform for detection comes from the most relativistic part of the dynamics: the last few cycles of the adiabatic inspiral, the plunge and the merger. Since LIGO is currently taking data at the expected sensitivity, it becomes urgent to have accurate template waveforms for detection. In the most general, spinning case, these waveforms are complicated functions of the initial masses m_1 and m_2 and the spins \mathbf{S}_1 and \mathbf{S}_2 of the two constituent black holes. Due to the multi-dimensionality of the parameter space, it seems impossible for state-of-the-art numerical simulations to densely sample this parameter space. This motivates a renewed effort for developing *analytical* methods towards computing the huge banks of accurate template waveforms needed to densely cover the parameter space.

As far as we know, the first estimate of the complete waveform (covering inspiral, plunge, merger and ring-down) of a coalescing, non-spinning black hole binary was made in 2000 [1], on the basis of a new analytical approach to the general relativistic two-body dynamics, the *Effective-One-Body* (EOB) approach [2]. At the time, no reliable numerical simulations of coalescing black hole binaries were yet available. This EOB-based estimate used a 2.5 post-Newtonian (PN) accurate description

of the dynamics (the only one available at the time¹) and a quadrupole-type “restricted waveform” approximation for the waveform down to a “matching radius” r_{match} where the two-black-hole system was replaced by a unique, ringing Kerr black hole. It was also argued that the matching radius r_{match} could be taken as the EOB-deformed “light ring”, r_{LR} , which was noticed to be very close to the point where the orbital frequency reached a maximum. As a first approximation, a complete waveform was computed by matching, at $r_{\text{match}} \simeq r_{\text{LR}}$, the inspiral-plus-plunge waveform to a ring-down waveform made of the least damped quasi-normal mode (QNM) of a Kerr black hole of mass and angular momentum corresponding to those of the relative dynamics at r_{match} . In other words, Ref. [1] was making the assumption that the *merger phase* of the two black holes was very brief, and did not correspond to any especially strong GW emission feature, but would simply smoothly connect the plunge behavior to the ringdown one.

In 2001, a combination of (rather short) full numerical simulations with a “close-limit” approximation [4] led to the first numerical estimate of the waveform emitted by the plunge from the ISCO, followed by merger and ringdown [5, 6]. Very recent breakthroughs in numerical relativity simulations have finally made accessible a

¹ This EOB waveform estimate was later updated by taking into account the more accurate 3.5 PN dynamics, as well as by considering spinning black holes [3].

much more precise knowledge of the waveforms generated by the merger of two black holes of comparable masses m_1 and m_2 , possibly with spin. These results have been obtained by different groups with different approaches, and exhibit convincing internal convergence and a nice mutual consistency [7, 8, 9, 10, 11, 12, 13, 14, 15, 16]. The availability of reliable numerical results makes it urgent to compare analytical and numerical approaches for (i) understanding in depth the physics that is involved in the process and thus (ii) completing the currently available analytical knowledge of the problem with the “missing” non-perturbative physics provided by numerical relativity simulations. Several different ways of combining the knowledge acquired through analytical and numerical methods have been recently explored, such as the use of “hybrid” signals made by stitching together an inspiral PN-type waveform to a NR merger one [17, 18], or the study of whether some simple multiparameter (BCV-type [19]) analytical waveform can have sufficiently large overlaps with hybrid signals. Our aim here is different. We wish, ultimately, to construct *high-accuracy* purely analytical template waveforms, depending only on physical parameters, and covering the full process: inspiral, plunge, merger and ringdown; by high-accuracy we mean that their phasing (and possibly their amplitude too) would be very close to the true phasing, uniformly, to a few percent. Let us recall that it is convenient (following the terminology of Ref. [20]) to distinguish *effectual* and *faithful* templates: effectual templates are defined by the property of having sufficiently large (say $\geq 96.5\%$) overlaps with the expected “real” signals, *after maximization over all (kinematical, dynamical, and possibly fudge) parameters*. Effectual templates maybe useful tools for *detecting* real signals, but they might lead to large biases in the measurement of the physical parameters of the system. By contrast, faithful templates are defined by the property of having not only large overlaps, but also of being so “close” to the real signals that the overlap between the template and the real signal is maximized for values of the parameters which are very close to the real ones (“small biases”). Recent “first order” comparisons between full numerical relativity waveforms and EOB-based waveforms have already established that EOB waveforms can be *effectual* (overlaps $\geq 96.5\%$) over the full mass range of interest for GEO/LIGO/VIRGO, say a total mass $M = m_1 + m_2$ between 10 and 120 solar masses [17, 21]. Our main aim will be to prove that EOB-based waveforms can also be *faithful* over the full mass range of interest. Our methodology for achieving this aim is to improve the current waveform implementations [1, 3, 17, 21] of the EOB approach [1, 2, 22, 23, 24] by understanding, element by element, the physics behind each feature of the waveform, and by comparing EOB-based waveforms with “exact” waveforms obtained by numerical relativity approaches. In the present paper, we shall tap the information contained in small-mass-ratio waveforms. [A preliminary version of our results was reported in [25].]

Indeed, the limiting case $m_1 m_2 \ll (m_1 + m_2)^2$ constitutes a “clean laboratory” where many subtle physical issues can be studied in detail (and by means of rather light numerical tools), without the complications entailed by the current three-dimensional numerical simulations (residual eccentricity, numerical noise,...). We rely on the recently developed numerical waveform computations à la Regge-Wheeler-Zerilli in Ref. [26]. Note that we consider non-spinning inspiralling systems circularized by radiation reaction.

The various improvements in the EOB waveform construction that we shall address here concern: (i) an improved analytical expression for the $((\ell, m) = (2, 2))$ waveform which includes a resummation of the tail effects, and a 3PN-accurate “non-linear” amplitude correction, (ii) the inclusion of non-quasi-circular corrections to the waveform, (iii) a comparative study of the two radiation reaction expressions during the plunge that have been proposed ([1] versus [24]), (iv) the inclusion of non-quasi-circular corrections to radiation reaction, and (v) an improved treatment of the matching between the plunge and ring-down waveforms (which takes into account a new understanding of the importance of the number of QNMs, the sign of their frequencies, and the length of the interval on which the matching is done). We shall show that the resulting improved implementation of the EOB approach yields very faithful waveforms whose amplitude and phase agree remarkably well with the “exact” ones: in particular, the EOB phasing differs from the “exact” one by less than $\pm 1.1\%$ of a cycle over the whole process.

This paper is organized as follows. In Sec. II we recall the EOB construction for the relative dynamics of the binary system and specify it to the small mass ratio limit. In Sec. III we discuss the computation of the GW emission and we focus on the comparison between different expressions of radiation reaction. Sec. IV introduces our “best” EOB-type waveform for the transition from inspiral to plunge and shows that it is an excellent approximation to the “actual” waveform. Some conclusions are presented in Sec. V.

II. EOB RELATIVE DYNAMICS

In this section we recall the EOB non-perturbative construction of the two-body dynamics including a radiation reaction force and then specify it to the small mass limit. The EOB approach to the general relativistic two-body dynamics is a *non-perturbatively resummed* analytic technique which has been developed in Refs. [1, 2, 3, 22, 23, 24]. This technique uses, as basic input, the results of PN theory, such as: (i) PN-expanded equations of motion for two point-like bodies, (ii) PN-expanded radiative multipole moments, and (iii) PN-expanded energy and angular momentum fluxes at infinity. For the moment, the most accurate such results are the 3PN conservative dynamics [27, 28], and the 3.5PN

energy flux [29, 30, 31]. Then the EOB approach “packages” this PN-expanded information in special *resummed* forms which extend the validity of the PN results beyond the expected weak-field-slow-velocity regime into (part of) the strong-field-fast-motion regime. At the practical level, the result of this “packaging” is that the complicated PN-expanded relative dynamics, (in the center of mass frame) of a binary system of masses m_1 and m_2 is mapped into the simpler (essentially geodesic) dynamics of a particle of mass $\mu = m_1 m_2 / (m_1 + m_2)$ moving in some effective background geometry (in Schwarzschild gauge)

$$ds^2 = -A(r)dt^2 + B(r)dr^2 + r^2(d\theta^2 + \sin^2\theta d\varphi^2). \quad (1)$$

Here and below we work with dimensionless reduced variables $r = R/M$ and $t = T/M$, with $M = m_1 + m_2$; (r, θ, φ) are polar coordinates in the *effective* problem that describe the relative motion. The dynamics of the effective particle is described by a Hamiltonian $H_{\text{EOB}}(M, \mu)$ and a radiation reaction force $\mathcal{F}_{\text{EOB}}(M, \mu)$. In the general comparable-mass case H_{EOB} has the structure $H_{\text{EOB}}(M, \mu) = M\sqrt{1 + 2\nu(\hat{H}_\nu - 1)}$ where $\nu \equiv \mu/M \equiv m_1 m_2 / (m_1 + m_2)^2$ is the symmetric mass ratio. In the test mass limit that we are considering, $\nu \ll 1$, we can expand H_{EOB} in powers of ν . After subtracting inessential constants we get a Hamiltonian per unit (μ) mass $\hat{H} = \lim_{\nu \rightarrow 0} (H_{\text{EOB}} - \text{const.}) / \mu = \lim_{\nu \rightarrow 0} \hat{H}_\nu$. It is convenient to replace the Schwarzschild radial coordinate R by the Regge-Wheeler tortoise coordinate $R_* = R + 2M \log[R/(2M) - 1]$, and, correspondingly, the radial momentum P_R by the conjugate momentum P_{R_*} of R_* . Then the (specific) Hamiltonian reads [26]

$$\hat{H} = \sqrt{A(r) \left(1 + \frac{p_\varphi^2}{r^2} \right) + p_{r_*}^2}. \quad (2)$$

Here we have introduced dimensionless variables $r \equiv R/M$, $r_* \equiv R_*/M$, $p_{r_*} = P_{R_*}/\mu$ and $p_\varphi = P_\varphi/(\mu M)$. In the $\nu \rightarrow 0$ limit, we have that $A(r) = B(r)^{-1} = 1 - 2/r$. We have used the tortoise canonical pair (r_*, p_{r_*}) instead of the “traditional” one (r, p_r) in the Hamiltonian for two related reasons. On the one hand, p_{r_*} has a finite limit when r tends to the zero of $A(r)$ ($r = 2$, the event horizon), while p_r diverges there². On the other hand, since one of our goal is to compute the gravitational wave signal from the relative dynamics, it is very useful to have the (radial-delta-function) source moving quasi-uniformly towards $-\infty$ on the doubly-infinite r_* axis, rather than exponentially slowing down and getting

² This divergence leads, in particular, to numerical problems in the source of the Regge-Wheeler-Zerilli equation: some “exact” analytical cancellations that are explicit when expressing the source in terms of p_{r_*} (which stays finite), become implicit when using p_r and numerically tend to yield a problematically divergent source.

stuck at $r = 2M$ (this allows us to cut-off more smoothly the radial motion after some time). For details of our numerical implementation see [26].

Hamilton’s canonical equations for $(r, r_*, p_{r_*}, p_\varphi)$ in the equatorial plane ($\theta = \pi/2$) yield

$$\frac{dr_*}{dt} = \frac{p_{r_*}}{\hat{H}}, \quad (3)$$

$$\frac{dr}{dt} = \frac{A}{\hat{H}} p_{r_*} \equiv v_r, \quad (4)$$

$$\frac{d\varphi}{dt} = \frac{A}{\hat{H}} \frac{p_\varphi}{r^2} \equiv \Omega, \quad (5)$$

$$\frac{dp_{r_*}}{dt} = -\frac{r-2}{r^3 \hat{H}} \left[p_\varphi^2 \left(\frac{3}{r^2} - \frac{1}{r} \right) + 1 \right], \quad (6)$$

$$\frac{dp_\varphi}{dt} = \hat{\mathcal{F}}_\varphi. \quad (7)$$

Note that the quantity Ω is dimensionless and represents the orbital frequency in units of $1/M$. In these equations the extra term $\hat{\mathcal{F}}_\varphi$ (of order $O(\nu)$) represents the non conservative part of the dynamics, namely the radiation reaction force. During the *quasi-circular inspiral*, a rather accurate expression for $\hat{\mathcal{F}}_\varphi$ is the following Padé-resummed form

$$\hat{\mathcal{F}}_\varphi^K \equiv \frac{\mathcal{F}_\varphi^K}{\mu} = -\frac{32}{5} \nu \Omega^{7/3} \frac{\hat{f}_{\text{DIS}}(v_\Omega)}{1 - \sqrt{3}v_\Omega}, \quad (8)$$

which is expressed in terms of the PN ordering parameter $v_\Omega \equiv \Omega^{1/3}$. In this expression, the function \hat{f}_{DIS} denotes the “factored flux function” of [20] (scaled to the Newtonian (quadrupole) flux), taken here in the $\nu \rightarrow 0$ limit. Ref. [1] (in the comparable mass case) assumed that the analytical continuation of the expression (8) might still be a sufficiently accurate description of radiation reaction effects during the *plunge*. On the other hand, the authors of Ref. [24] pointed out that the expression (8) assumed the continued validity of the usual Kepler law $\Omega^2 r^3 \simeq 1$ during the plunge. [This is why we label the expression (8) with a superscript K , for Kepler.] They, however, emphasized that the Kepler combination $K = \Omega^2 r^3$ significantly deviates from one after the crossing of the Last Stable (circular) Orbit (LSO), to become of order of 0.5 at the light ring. Ref. [24] went on to argue for a different expression for the radiation reaction, say $\hat{\mathcal{F}}_\varphi$ (without any superscript) that does not assume Kepler’s law. In the $\nu \rightarrow 0$ limit this new expression reads

$$\hat{\mathcal{F}}_\varphi \equiv \frac{\mathcal{F}_\varphi}{\mu} = -\frac{32}{5} \nu \Omega^5 r^4 \frac{\hat{f}_{\text{DIS}}(v_\varphi)}{1 - \sqrt{3}v_\varphi}. \quad (9)$$

where the ordering PN parameter is given by the azimuthal velocity $v_\varphi = r\Omega$. Note that the essential difference between the two possible expressions for the radiation reaction is that $\hat{\mathcal{F}}_\varphi^K \propto \Omega^{7/3}$, while $\hat{\mathcal{F}}_\varphi \propto \Omega^5 r^4$. For simplicity, in both possible expressions for the radiation reaction our current estimate of \hat{f}_{DIS} is obtained by Padé approximating the 2.5 PN results, a procedure

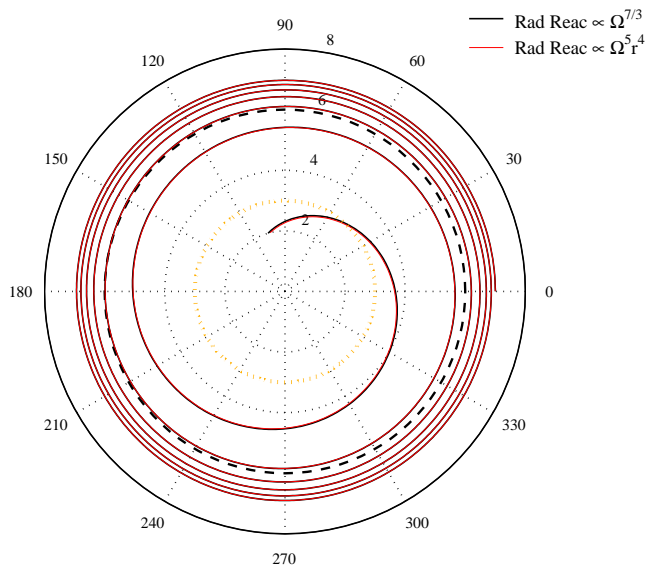


FIG. 1: Relative dynamics for $\nu = \mu/M = 0.01$ and initial separation $r = 7$. The plot shows the (nearly indistinguishable) trajectories with $\hat{\mathcal{F}}_\varphi^K$ (black line) and with $\hat{\mathcal{F}}_\varphi$ (red line). The dashed circle indicates the LSO (which is crossed at the dynamical time $t/2 \simeq 240$). The light ring (at $r = 3$), near which the plunge waveform will be matched to a ring-down one, is indicated (dotted circle). It is crossed at the dynamical time $t/2 \simeq 300$ [26].

that has already been shown to be quite robust versus “exact” numerical results in [20].

Let us finally comment on the numerical values of the parameter ν that we shall consider. First, we should consider values such that the ν -dependent corrections in the two-body effective Hamiltonian \hat{H}_ν , i.e. the ν -dependent contributions in the EOB metric functions such as $A(r) = 1 - 2u + 2\nu u^3 + \dots$ (where $u \equiv 1/r$), are indeed numerically negligible. However, we do not wish to consider too small values of ν . Indeed, the present study of the inspiral, plunge and merger of a mass μ into a Schwarzschild black hole of mass M is intended as a toy model of the coalescence of two comparable-mass black holes. We therefore wish to minimize the quantitative difference between these two types of inspiralling motions. In particular, it has been shown in Ref. [1] that the number of orbits during the comparable-mass plunge was roughly $\sim (4\nu)^{-1/5}$, i.e. a number of order one when $m_1 = m_2$ (i.e. $\nu = 1/4$). We should *not* therefore consider values of ν so small as to make $(4\nu)^{-1/5}$ much larger than one. As a compromise we shall always consider here the value $\nu = 0.01$, which gives only $\sim (4\nu)^{-1/5} \simeq 1.9$ orbits during the plunge (as will indeed appear in Fig. 1 below).

III. REGGE-WHEELER-ZERILLI WAVEFORMS

Following what we did in [26], the computation, à la Regge-Wheeler-Zerilli³ of the gravitational waveform in the $\nu \rightarrow 0$ limit needs three separate steps: (i) to initialize the system (3)-(7), (ii) to integrate it in time and (iii) to solve the Regge-Wheeler and Zerilli-Moncrief equations as an initial value problem, with source terms driven by the particle dynamics. In practice, once the dynamics is computed, one needs to solve (for each multipole (ℓ, m) of even (e) or odd (o) type) the following couple of decoupled partial differential equations

$$\partial_t^2 \Psi_{\ell m}^{(e/o)} - \partial_{r_*}^2 \Psi_{\ell m}^{(e/o)} + V_\ell^{(e/o)} \Psi_{\ell m}^{(e/o)} = S_{\ell m}^{(e/o)} \quad (10)$$

with source terms $S_{\ell m}^{(e/o)}$ linked to the dynamics of the binary. A thorough discussion of the analytical and numerical details of our approach has been given in Ref. [26], so that it is not necessary to repeat it here. We only recall that the initial condition for the relative dynamics is given as in [26], notably by specifying a non-zero initial value for p_{r_*} (“post-adiabatic” approximation). In addition, the gauge-invariant functions $\Psi_{\ell m}^{(e/o)}$ are proportional to the actual GW polarization amplitudes, and so their knowledge encodes the complete information about energy, momentum and angular momentum losses.

A. Angular momentum loss

Let us consider the relative dynamics of a particle of mass $\mu = 0.01M$ plunging from $r = 7$. The relative orbit (for both choices of radiation reaction) is shown in Fig. 1. The dashed circle indicates the LSO, which is crossed at $t/2 \simeq 240$, while the dotted circle indicates the light ring (LR), which is crossed at $t/2 \simeq 300$ [26]. The first point we want to discuss is the comparison (and contrast) between the two expressions of the angular momentum loss mentioned above, the “usual” Keplerian one $\hat{\mathcal{F}}_\varphi^K$ of Eq. (8) and $\hat{\mathcal{F}}_\varphi$ of Eq. (9). These two expressions are equivalent during the inspiral due to the validity of Kepler’s law $\Omega^2 r^3 = 1$ along circular orbits, but they start strongly deviating from each other after the crossing of the LSO. We wish to know how they compare to some sort of “exact” angular momentum flux during the plunge, and whether one of them is to be preferred.

Let us now be precise in which respect we can compute an “exact” result for the angular momentum loss during the plunge. We recall that via Eq. (17) of Ref. [26] one can compute the instantaneous angular momentum flux at infinity dJ/dt (as a sum of multipoles) from $\Psi_{\ell m}^{(e/o)}$. We have done this for both $\hat{\mathcal{F}}_\varphi^K$ and $\hat{\mathcal{F}}_\varphi$ including all

³ i.e., by computing the metric perturbations of a Schwarzschild spacetime by means of a multipolar decomposition. See for example [32] and references therein.

the multipoles of the radiation up to $\ell = 4$. The solid lines in Fig. 2 refer to this computation. There, dJ/dt is extracted at $r^{\text{obs}} = 500$ and is shown versus observer's retarded time $u = M(t^{\text{obs}} - r_*^{\text{obs}}) + \Delta u$, where one shifts the retarded time u by a constant so as to best fit (during the early inspiral) the dynamical time t which enters as the argument of the local angular momentum loss of the source, i.e. the radiation reaction $\hat{\mathcal{F}}_\varphi^K(t)$ or $\hat{\mathcal{F}}_\varphi(t)$. We use $\Delta u = 0.4M$. The labelling “Flux with $\propto \Omega^{7/3}$ Rad Reac” indicates the outcome of a dynamics with $\hat{\mathcal{F}}_\varphi^K$ (black line), while “Flux with $\propto \Omega^5 r^4$ Rad reac” refers to a dynamics using $\hat{\mathcal{F}}_\varphi$ (red line). Fig. 2 shows that the differences in the fluxes at infinity are really tiny. In that sense, we know with good accuracy (assuming balance between losses at infinity and local losses) what should be the “exact” (local) angular momentum loss of the system. By contrast, the two dashed lines in Fig. 2 represent the two analytically-assumed local angular momentum losses; i.e., the two radiation reaction terms $\hat{\mathcal{F}}_\varphi^K(t)$ or $\hat{\mathcal{F}}_\varphi(t)$. The good news is that they agree quite well with the “exact” result during not only the inspiral, but also a fair fraction of the plunge (which starts at $u/2M \simeq 240$). However, the bad news is that they start differing significantly from the exact result (as well as from each other) during the later part of the plunge (say, after $u/2M \simeq 290$, remembering that the matching to ring-down will be done around $u/2M \simeq 300$, which corresponds to light-ring crossing). The “usual” Kepler-based radiation reaction $\hat{\mathcal{F}}_\varphi^K$ is too large (as anticipated in Ref. [24] which pointed out that $K = \Omega^2 r^3$ sharply decreases during the plunge, if we notice that the ratio $\hat{\mathcal{F}}_\varphi^K/\hat{\mathcal{F}}_\varphi \simeq K^{-4/3}$), while the hopefully better radiation reaction $\hat{\mathcal{F}}_\varphi$ turns out to be somewhat too small towards the end of the plunge. On the other hand, the near coincidence of the two corresponding fluxes at infinity shows that the “analytical uncertainty” in the radiation reaction does not matter much for computing the waveform. This confirms, and makes more quantitative, the finding of [1, 33] that, after the crossing of the LSO, the relative motion is essentially *quasi-geodesic*; i.e., relatively little influenced by the radiation-reaction force.

The physics behind the differences between the “analytical” and “exact” angular momentum fluxes (as well as between the two analytical ones) lies in the presence of *non-quasi-circular* (NQC) effects during the plunge phase. During the adiabatic inspiral one takes advantage of the quasi-circularity (QC) of the motion to operate *two separate simplifications*: (a) one neglects the terms proportional to dr/dt , and (b) one neglects the terms proportional to d^2r/dt^2 , which, by using the equations of motion, give (modulo the square of dr/dt) terms proportional either to $v^2 - 1/r$ (“virial combination”), or to $\Omega^2 r^3 - 1$ (“Kepler combination” minus 1). During the plunge, both simplifications become less and less valid so that one should correct any QC-derived expression by terms proportional to powers of the two basic dimensionless NQC ratios $(dr/dt)/(\Omega r)$ and $(1/r - v^2)/v^2$. When

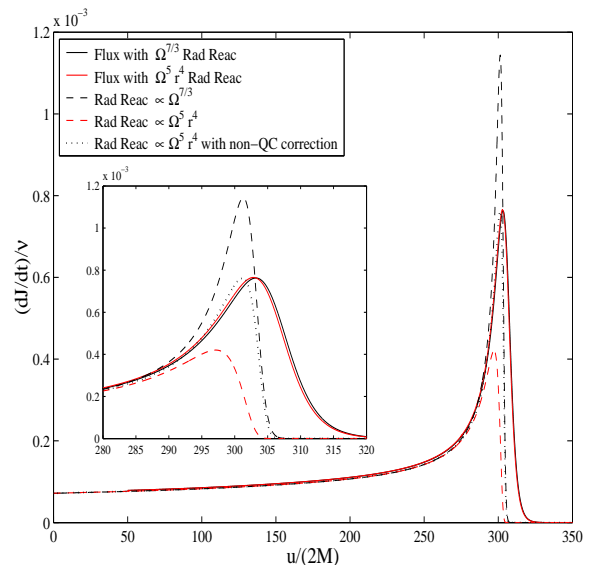


FIG. 2: Comparison between various angular momentum losses: GW fluxes at infinity (solid lines; computed à la Regge-Wheeler-Zerilli including up to $\ell = 4$ radiation multipoles, using two types of radiation reaction in the driving dynamics: ‘K’ (black) or ‘not K’ (red)); or mechanical angular momentum losses: $(dJ/dt)^K = -\hat{\mathcal{F}}_\varphi^K$ (hyphenated black lines), $dJ/dt = -\hat{\mathcal{F}}_\varphi$ (hyphenated red lines). The dotted line refers to the mechanical losses with non-quasi-circular corrections. See text for discussion.

considering a time-even NQC correcting factor, it should have the general form

$$f^{\text{NQC}} = 1 + a \left(\frac{p_{r_*}}{r\Omega} \right)^2 + a' \left(\frac{1}{K} - 1 \right) + \dots, \quad (11)$$

where we used the same “Kepler combination” $K \equiv \Omega^2 r^3$ as before. In our present case, we physically expect the presence of such a time-even NQC⁴ factor in the radiation reaction. As we expect (from the usual quadrupole formula, as well as from the well-known fact that orbital eccentricity tends to *increase* the flux of angular momentum) that the NQC factor in the radiation reaction should be *larger than one*, we conclude that the “improved” radiation reaction expression $\hat{\mathcal{F}}_\varphi$ proposed in [24] is a physically more appealing starting point for applying such a NQC correcting factor. In addition, as, pragmatically speaking, the two types of terms parametrized by a and a' in Eq. (11) above behave in a roughly similar way during the plunge (they are both positive and they both increase), we can try, in first approximation, to use only one of them, say the first one parametrized by a .

In Fig. 2 we show (as a black dotted line labelled “Rad Reac $\propto \Omega^5 r^4$ with non-QC corrections”) the evolution of

⁴ Note that we can henceforth view NQC as meaning either *non-quasi-circular* or *next-to-quasi-circular*.

the NQC-corrected radiation reaction

$$\hat{\mathcal{F}}_\varphi^{\text{NQC}} \equiv \hat{\mathcal{F}}_\varphi \left(1 + a^{RR} \frac{p_{r_*}^2}{(r\Omega)^2} \right) \quad (12)$$

with the numerical value $a^{RR} = +2.9$ (fixed by eye). We see how such a simple (and physically reasonable, because larger than one) NQC factor suffices to have a good agreement between a “NQC-corrected analytical radiation reaction” and the “exact” angular momentum flux dJ/dt up until the light-ring, that is crossed at $u/(2M) \approx 300$. This gives our first instance of the aim of the present paper: to better understand (by comparing to “exact” numerical results) the “missing physics” in some first-order analytical expression, and then to use this improved understanding to further improve the starting analytical expression. Note that, for any starting QC expression X that one wishes to correct, it is in principle possible to compute in General Relativity the “real” NQC correcting factor f_X^{NQC} , of the form (11) with some analytically computable coefficients a_X, a'_X , etc. Note, however, that one expects these coefficients to become (when considering PN corrections) functions of $1/r$ and other dynamical variables. As in several other known cases, one expects that these PN corrections might significantly affect the “effective” numerical value of the coefficients a_X, a'_X , etc needed for a good representation of the considered quantity during the plunge. It would be interesting to have analytic (at least 1PN-accurate) results on the coefficients $a_{\mathcal{F}}^{RR}, a'_{\mathcal{F}}{}^{RR}$ to compare them with our presently “experimental” estimate $a_{\text{effective}}^{RR} = +2.9$.

B. Exact waveforms

Let us now consider the waveforms obtained by numerically integrating the Regge-Wheeler-Zerilli equation (10), with a source corresponding to the plunging dynamics discussed above, with the $\hat{\mathcal{F}}_\varphi$ radiation reaction (we have checked that the NQC-improved radiation reaction (11) introduces only very minor changes in the waveform). For the most relevant multipolarity ($\ell = m = 2$, with even parity), the resulting “exact” waveforms (denoted $\Psi_{22}^{(\text{exact})}$, or sometimes $\Psi_{22}^{(e)}$) are displayed in Fig. 3. The left panel of the figure exhibits (black lines) the real (top) and imaginary (bottom) part of $\Psi_{22}^{(\text{exact})}$ (normalized as in [32]). The waveforms are extracted at $r_{\text{obs}} = 500$ and are shown versus the (shifted) observer retarded time. They exhibit the usual “chirp-like” structure corresponding to the inspiral, and end up with the black hole QNM ringing.

The most useful information about the dynamics of the merger hidden in the (exact or analytical) waveform can be extracted by inspection of the corresponding instantaneous gravitational wave frequency. Since Ψ_{22} is a

complex number, this quantity is computed as

$$M\omega_{22} = \hat{\omega}_{22} \equiv -\Im \left(\frac{\dot{\Psi}_{22}}{\Psi_{22}} \right), \quad (13)$$

where \Im indicates the imaginary part and the overdot stands for d/dt . The *exact* $\hat{\omega}_{22}$ is shown as a black solid line in the right panel of Fig. 3. In the same plot we also include, as a blue line, twice the orbital frequency Ω (which is the zeroth-order analytical prediction coming from any “standard quadrupole approximation”). This plot shows that $\hat{\omega}_{22}^{(\text{exact})} \approx 2\Omega$ during the inspiral and most of the plunge (the LSO is crossed at $u/(2M) \simeq 240$). It is only when the (relative) radius gets quite near the light-ring value $r = 3$ (at $u/(2M) \approx 300$, indicated by a green dashed vertical line) that the two frequencies start deviating from each other. While the doubled orbital frequency 2Ω reaches a maximum equal to $2\Omega_{\text{max}} = 0.2703$ very near the light ring⁵ and then exponentially decreases, the exact GW frequency $\hat{\omega}_{22}$ keeps growing after the light ring until it saturates and oscillates around the fundamental QNM frequency of the black hole, $M\omega_{220} = 0.3736715$ [34, 35]. The oscillation in the GW frequency around the fundamental QNM frequency is (essentially) due to the superposition of both *positive*-⁶ and *negative*-frequency excitations in the ring-down waveform.⁷ Let us mention that this kind of behavior of $M\omega_{\ell m}^{(e/o)}$ (odd and even-parity GW frequencies) is absolutely general and the amplitude of the oscillation depends on m [36].

The fact that the *amplitude* of the frequency oscillation in the right panel of Fig. 3 is quite small then means that the positive-frequency mode is excited with a much larger coefficient than the negative-frequency one. In view of our general aim of understanding all the separate physical elements crucially entering the final waveform, it is interesting to explain what is the basic underlying physics behind this large dissymmetry in the excitation coefficients of the positive-frequency and negative-frequency modes (we have checked that this dissymmetry extends to the first few overtones above the fundamental QNM mode). Though this basic physics can be de-

⁵ It is easy to see from the Hamiltonian equation (5) why this is so: neglecting the relatively slow variations of the angular momentum and the energy, Ω vary proportionally to the ratio $A(r)/r^2$ which is precisely the effective radial potential for photon (or ultra-relativistic) circular orbits.

⁶ As in Quantum Field Theory we call *positive* frequency a mode $\propto e^{-i\omega t}$ with $\omega > 0$. We also use for the QNMs (see below) the notation $\propto e^{-\sigma t}$. In this notation, the positive frequency fundamental mode has $\sigma_0^+ = \alpha_0 + i\omega_0$, where ω_0 indicates the frequency and α_0 the damping time of the fundamental mode, while the negative frequency one has $\sigma_0^- = \alpha_0 - i\omega_0$.

⁷ Evidently, had we initialized the dynamics with the opposite sign of p_φ , i.e., the particle inspiralling *clockwise* and not *counter-clockwise*, we would have obtained a mirror-reflected result, with the negative frequency modes being more excited than the positive frequency ones.

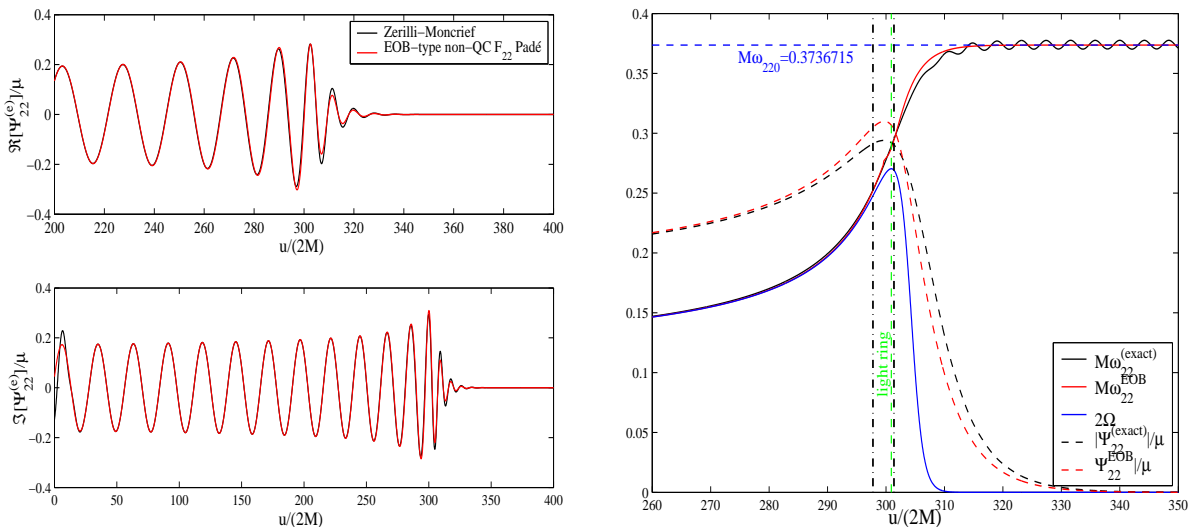


FIG. 3: *Left panel:* Quadrupole waveforms ($\ell = m = 2$, even parity): exact Zerilli-type (black line) and “matched” improved EOB-type (red line). *Right panel:* exact and matched-EOB modulus and instantaneous gravitational wave frequency. The blue line displays twice the orbital frequency Ω . The two vertical dash-dot lines mark the ends (at 297.8 and 301.4) of our matching interval (which is centered, at 299.6 on the maximum of the modulus, and which includes the light ring, at 300.9).

scribed in terms of equations, it is best understood by means of some diagrams. One should have in mind that solving the Regge-Wheeler-Zerilli equation (10) means essentially considering a point-source (moving along the radial axis) whose “strength” oscillates proportionally to $\exp[-im\varphi(t)]$ (with $m = +2$ in the present case) and which is located at a time-dependent radius $r_*(t)$. If the radial velocity is small with respect to the azimuthal velocity (as is true during most of the plunge) we can think of a source with an adiabatically varying frequency $m\Omega(t)$ located at the adiabatically varying radius $r_*(t)$. Replacing this behavior in equation (10) allows one to approximately replace the repeated time derivative by the square of the instantaneous source frequency, i.e. by a factor $(-im\Omega(t))^2 = -(m\Omega(t))^2$. This yields a Schrodinger-type (radial) equation with effective potential $V_\ell^{(e/o)}(r_*) - (m\Omega(t))^2$. In the upper panel of Fig. 4, we compare the evolution, as a function of dynamical time t , of the square roots of the two contributions to this effective radial potential: $\sqrt{V_\ell^{(e/o)}(r_*(t))}$ and $m\Omega(t)$ (for the case $\ell = m = 2$). We see that the $(m\Omega(t))^2$ term is always significantly smaller than the $V_\ell^{(e/o)}(r_*(t))$ one. This means that during all the plunge (including at the end, when $\Omega(t)$ reaches its maximum value), we can think (in first order) in terms of a *near-zone* approximation, where we can neglect $(2\Omega(t))^2$ and compute the asymptotic waveform by convolving the source by a solution of the static, radial Regge-Wheeler-Zerilli equation. One can check that this leads essentially to the usual (Schwarzschild-coordinate) quadrupole formula for the waveform. In this approximation there is strictly no excitation of the QNM modes by the adiabatically vary-

ing source. One therefore concludes (following the line of reasoning of Ref. [24] where it was explained how a certain type of oscillating integral which exponentially vanishes in the adiabatic approximation acquired a non-zero value due to a localized non-adiabatic behavior of the integrand) that the QNM modes will be excited essentially only around the maximum of the exciting frequency $m\Omega(t)$, because this is the moment when the source excitation is *non-adiabatic*. Looking now at the bottom panel of Fig. 4, we see the trajectory of the exciting frequency on the *positive* real axis, from zero up to the maximum $2\Omega_{\max} = 0.2703$. The black dots in the complex frequency plane represent the first QNM modes of a Schwarzschild black hole. One understands intuitively (and this can be put in equations similar to those derived in [24]) that the amount of excitation, by the non-adiabatic behavior of the excitation frequency near its maximum, of the various QNM modes will primarily depend on their “distance” to the critical (real) exciting frequency $+2\Omega_{\max} = +0.2703$. This reasoning indicates that the QNM modes which will be primarily excited are the first few *positive frequency* modes, i.e. those appearing on the right part of the bottom panel of Fig. 4. Summarizing in slightly different physical terms, we can think of the black hole as a resonating object having the resonance spectrum showed in Fig. 4. When the source varies adiabatically, so that it corresponds to a nearly pure frequency $+m\Omega$ which is much *smaller* than any of the resonance frequencies it excites only negligibly the resonance modes. However, when the source varies non-adiabatically (near its maximum frequency), its Fourier transform contains a halo of frequencies (due to non-adiabaticity) centered around the instantaneous

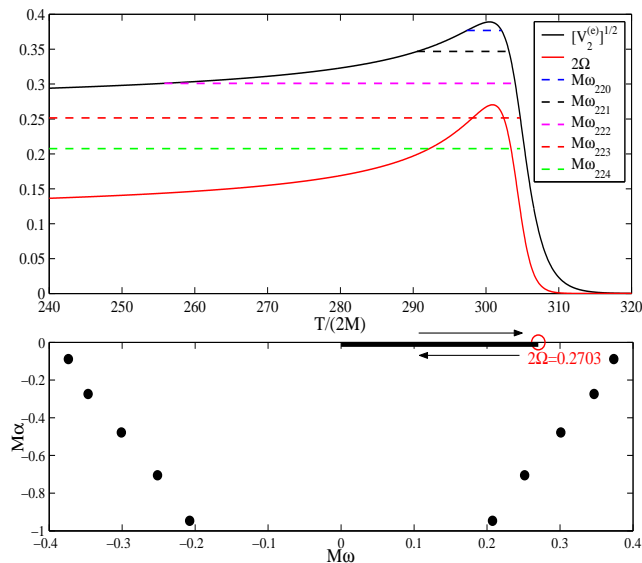


FIG. 4: Illustration of some of the important physical features of the excitation of quasi-normal modes by a small-mass-ratio coalescing binary system. The upper panel shows that, during all the plunge, one remains in a “quasi-stationary” near-zone regime (which does not excite QNMs). The crucial feature which can excite the QNMs is the *non-adiabaticity* of the evolution of the exciting orbital frequency near its maximum (similarly to Ref. [24]). The lower panel illustrates why the (rather short) non-adiabatic behavior of $2\Omega(t)$ near its maximum preferentially excites the positive-frequency QNMs.

frequency, and this halo can now “extend the reach” of $+m\Omega_{\max}$ and thereby excite the black hole resonances which lie within this “halo” (i.e. the first few QNM modes whose frequency has the *same sign* as $+m\Omega_{\max}$).

IV. EOB-TYPE APPROXIMATE WAVEFORMS

A. Methodology: a matched waveform

Let us now turn to the construction of complete EOB-type gravitational waveforms obtained by *matching* an analytical *inspiral-plus-plunge* waveform to a *ring-down* one. For the reasons explained above, the crossing of the light ring (actually the non adiabatic behavior around the moment when $\Omega(t)$ reaches it maximum) corresponds to an abrupt triggering of the QNMs of the black hole (this was realized long ago [37] for the case of the radial plunge). The EOB approach takes into account this abrupt change in the underlying physics by an abrupt change in the analytical description of the system: before the crossing of the light ring one describes the binary system as two point masses with EOB relative dynamics, while after the crossing one replaces the binary system by a single distorted black hole (as in the “close-limit” approximation of colliding black holes [4]). As we were mentioning in the introduction, at the practical

level this dual description implies that one should *match* together (around the light ring) a plunge waveform obtained with a *quadrupole-type* formula to a superposition of black hole QNMs. This general philosophy has already been implemented, with increasing sophistication in Refs. [1, 3, 17, 21, 24]. Our aim here is to further improve the implementation of the EOB approach by studying in detail each one of its building blocks, and by comparing the resulting analytical waveform to the *exact* numerical waveforms discussed above.

B. An improved, resummed 3PN-accurate inspiral-plus-plunge waveform.

We start by introducing here a new, improved EOB-type inspiral-plus-plunge waveform that goes beyond previous work in two directions: (i) it includes higher post-Newtonian (PN) effects which are *resummed* in a novel way (factorized formulation, exact resummation of tail effects, 3PN-resummed non-linear PN effects), and (ii) it includes non-quasi-circular (NQC) corrections that are expected to be relevant below the LSO. Details of our construction will be explained separately [36]. Up until the light ring ($r \gtrsim 3$), we use a $(\ell, m) = (2, 2)$ gravitational waveform defined by means of the following EOB-type improved quadrupole formula

$$\Psi_{22}^{\text{plunge}}(t) = -4\mu\sqrt{\frac{\pi}{30}}(r\Omega)^2 F_{22} \times \left\{ 1 + a\frac{p_{r*}^2}{(r\Omega)^2} + ib\frac{p_{r*}}{r\Omega} \right\} e^{-2i\varphi}. \quad (14)$$

Here, F_{22} includes four types of PN effects, while the braces represent NQC corrections. The standard quadrupole formula (for a point-particle source in quasi-circular motion) corresponds to the case where $F_{22} = 1$ and $a = b = 0$ (see e.g. [38]; the numerical coefficient $\sqrt{\pi/30}$ corresponds to our using the Zerilli-Moncrief even quantity $\Psi_{22}^{(e)}$).

The NQC factor added above (within braces) is more general than the general *time-even* NQC factor considered in (11) because we describe here non time-even NQC effects (as can easily be seen on the usual quadrupole formula written with two time-derivatives). The numerical coefficients a and b thus parametrize non-quasi-circular corrections to the modulus and to the phase of the wave. They will be fixed below by comparison to the “exact” Zerilli-Moncrief waveform. The novel F_{22} PN-improving factor is given as the product of four terms

$$F_{22}(t) = \hat{H}(t)T(2, 2\Omega(t))e^{i\delta_{22}(t)}f_{22}(x(t)). \quad (15)$$

This factorization of PN effects is, in itself, a new way of partially resumming PN effects (by contrast to usual representations of PN effects which mix the expansion of the four separate factors above). The first factor is

the ‘‘conserved’’ relativistic energy of the (effective) moving source. The second factor $T(2, 2\Omega)$ is the particularization to $\ell = m = 2$ of a function $T(\ell, k)$ (with $Mk \equiv \hat{k} = m\Omega$) that represents a ‘‘tail’’ correction, namely the contribution due to backscattering of (multipolar) waves off the background curvature. This factor is the exact resummation of an infinite number of ‘‘leading logarithms’’, and is derived, similarly to the work in Ref. [39], by using Coulomb wave functions. It is explicitly given by

$$T(\ell, k) = \frac{\Gamma(\ell + 1 - 2i\hat{k})}{\Gamma(\ell + 1)} e^{\pi\hat{k}} e^{2i\hat{k} \log(2kb_{\text{scale}})}, \quad (16)$$

where we shall take $b_{\text{scale}} = 2M$. $e^{i\delta_{22}}$ is an additional phase correction, with $\delta_{22} = 7\Omega/3$ to lowest PN order. The final factor $f_{22}(x)$ represents the remaining (essentially non-linear) PN effects. Using Ref. [40] it can be computed in the test-mass limit, during the inspiral, as a Taylor expansion in the PN-ordering parameter $x = 1/r = \Omega^2/3$. At 3PN⁸, it reads

$$f_{22}^{\text{Taylor}}(x) = 1 - \frac{43}{21}x - \frac{536}{189}x^2 + x^3 \left[\frac{21428357}{727650} - \frac{856}{105}\gamma - \frac{1712}{105}\log(2) - \frac{428}{105}\log(x) \right], \quad (17)$$

where $\gamma = 0.577216\dots$ is the Euler constant. To improve its convergence properties in the strong-field-fast-motion regime, expression (17) is further Padé resummed in a proper way.

When deriving the factor $f_{22}(x)$ during the inspiral phase, the argument x that it depends upon is ‘‘degenerate’’ in the sense that it can be expressed in various ways in terms of the dynamical variables of the system, namely: $x = v_\varphi^2 = (r\Omega)^2 = \Omega^2/3 = 1/r$. However, these various expressions start differing from each other during the plunge. This opens the issue of choosing the ‘‘best’’ dynamical expression for the PN-ordering argument x during the plunge, in the sense of giving the best approximation to the ‘‘exact’’ waveform (minimizing the need for NQC corrections). We have found that choosing $x = 1/r$ (the Newtonian gravitational potential) yields good results, and this is the choice we shall make here. We postpone to a further publication a thorough analysis of the effect of different x arguments, as well as the contrast between the Padé-resummed (that we shall use here) and Taylor-expanded versions of $f_{22}(x)$.

C. Ring-down waveform

After the crossing of the light ring, the EOB approach consists in replacing the two-body system by a single distorted black hole. At the level of waveforms, this means that one should *match*, around the light ring, the plunge waveform Eq. (14) to a *ring-down* one made of a superposition of ($\ell = 2, m = 2$) black hole QNMs, say

$$\Psi_{22}^{\text{ringdown}}(t) = \sum_n C_n^+ e^{-\sigma_n^+ t} + \sum_n C_n^- e^{-\sigma_n^- t}, \quad (18)$$

where $\sigma_n^\pm = \alpha_n \pm i\omega_n$ are the positive/negative complex QNM frequencies and C_n^\pm are the corresponding amplitudes. Here, α_n and ω_n indicate the damping time and the oscillation frequency of each mode respectively, and $n = 0, 1, 2, \dots, N - 1$ labels the overtone number ($n = 0$ denoting the fundamental mode).

In this paper we propose an improved treatment of the definition of the ring-down waveform Eq. (18), as well as of the matching to the plunge waveform Eq. (14). First, in view of both the numerical results and the theoretical arguments presented above, we know that the contribution of the positive-frequency modes to the waveform is much larger than that of the negative-frequency ones. Therefore, we can set $C_n^- = 0$ in first approximation. As a result, the instantaneous gravitational wave frequency $M\omega_{22}^{\text{EOB}} \equiv -\Im(\dot{\Psi}_{22}^{\text{EOB}}/\Psi_{22}^{\text{EOB}})$ of our ‘‘matched’’ ring-down waveform will grow until it reaches a ‘‘flat’’ saturation region, *without oscillations*. Though this is qualitatively slightly different from the behavior of the exact instantaneous frequency (see Fig. 3) we will see that this gives an excellent approximation to the phasing (and actually a better one that if one matches to both positive and negative modes in a democratic way).

Our problem is thus to determine the coefficients C_n^+ from the knowledge of $\Psi_{22}^{\text{plunge}}$ for $r \gtrsim 3$. Here again we introduce some significant improvements on previous implementations of the EOB philosophy, based on the knowledge acquired from detailed comparisons with our ‘‘exact’’ small-mass-ratio numerical results. A trivial improvement will consist in using a larger number N of QNMs (including the fundamental mode) than previous work. Instead of $N = 1$ [1, 3], $N = 2$ [24], or $N = 3$ [17, 21], we shall use here $N = 5$ (positive-frequency) quasi-normal modes (including the fundamental mode) [34, 35]. Our studies showed that $N = 5$ gives a significantly better fit than $N = 4$ or less, and that larger values of N yield only a rather marginal improvement.

D. Determining the next-to-quasi-circular (NQC) corrections to the plunge waveform.

First of all $\Psi_{22}^{\text{plunge}}$, Eq. (14), has two free parameters a and b that should be specified so to minimize the difference with the real signal. The presence of two separate NQC real parameters is useful because the waveform is a

⁸ We note that for $\nu \ll 1$ this series is known to higher PN orders. We truncate it here to the 3PN level which is the highest order at which we could (and did) derive it in the comparable-mass case. We leave to a future publication a detailed discussion of the derivation of these results.

complex number, and we wish to best fit both its modulus and its phase⁹. The *modulus* of the numerical waveform reaches a maximum at the (shifted) retarded time $u/(2M) = 299.6$ (i.e. just before the maximum of the orbital frequency, or the crossing of the light ring, which both occur near $u/(2M) = 300.9$). We can then constrain the NQC parameters a and b so as to ensure that the maximum of the modulus of the analytical waveform (14) sits on top of that of the exact modulus. Actually, we can even do this *analytically*. Using the quasi-geodesic approximate description of the plunge, and imposing that the modulus of the analytical waveform (14) is maximum at the light-ring gives, in first NQC approximation, the constraint $2a + b^2 = 1$. We then get a second constraint (mainly on the coefficient b) by requiring that the *slope* of the instantaneous analytical frequency $M\omega_{22}^{\text{plunge}}(t)$ be as close as possible to the exact one $M\omega_{22}(t)$ around the light ring. The two above requirements fix the values of the NQC parameters to be: $a = 0.438$ and $b = 0.355$. It is remarkable that these two numerical values (numerically determined, by trial and error, as best eye-fitting values) do satisfy quite accurately the (first-order) analytically determined constraint mentioned above: indeed, $2a_{\text{num}} + b_{\text{num}}^2 = 1.002$. This shows the power of the EOB approach for building a purely analytical *self-consistent* matched waveform, even in absence of knowledge about the exact signal.

E. Matching the inspiral-plus-plunge waveform to the ring-down one on a “comb”.

The last and most crucial new ingredient introduced here consists in *matching* the plunge and ring-down waveforms on a *finite time interval* $[t_m - \delta/2, t_m + \delta/2]$, instead of simply imposing the continuity of the two functions, and a certain number of their derivatives, at one moment t_{match} (as done in [1, 17, 21, 24]). We found that this matching on a finite interval (chosen in the immediate vicinity of light-ring crossing) was quite effective for accurately reproducing the smooth rise of the instantaneous GW frequency during the whole transition. More precisely, a good choice for the matching interval $[t_m - \delta/2, t_m + \delta/2]$ consists in putting its center t_m at the *maximum of the modulus* of $\Psi_{22}^{\text{plunge}}$, i.e. at $t/(2M) = 299.6$, and choosing his full length $\delta = \Delta t$ as $\delta/M \simeq 7.2$. The matching on the interval $[t_m - \delta/2, t_m + \delta/2]$ is most easily done by discretizing this matching interval into N (here $N = 5$) equally

spaced points, $[t_1, t_2, \dots, t_N]$ (with $t_1 = t_m - \delta/2$ and $t_N = t_m + \delta/2$) and requiring that the two complex functions (14) and (18) coincide at these N points. This gives N (linear) complex equations for the N complex unknowns C_n^+ . In other words we are using a ‘matching comb’.

F. Comparing analytical and numerical waveforms

Finally, we define our complete EOB matched waveform (from inspiral to ring-down) as

$$\Psi_{22}^{\text{EOB}}(t) \equiv \theta(t_m - t)\Psi_{22}^{\text{plunge}}(t) + \theta(t - t_m)\Psi_{22}^{\text{ringdown}}(t) \quad (19)$$

where $\theta(t)$ denotes Heaviside’s step function¹⁰.

The left panel of Fig. 3 compares the (real and imaginary parts of the) matched EOB-type waveform (19) (red line) obtained by means of the matching procedure explained above, to the “exact” numerical one (black line). The agreement between the two is clearly excellent. Note, in particular, how the inclusion of the novel 3PN-accurate correction factor F_{22} allows the analytical *inspiral* waveform to coincide in phase *and* in amplitude with the exact signal. As we shall illustrate below, Newtonian-accurate “restricted” waveforms do a much poorer job: though they describe the phasing rather accurately, they overestimate (already during the inspiral) the amplitude by a significant factor. To investigate further the quality of this agreement, we also plot the modulus of the waveforms and the instantaneous frequency (right panel of Fig. 3). One sees again on this figure the very accurate way in which the improved EOB signal reproduces both the frequency and the modulus of the exact signal during the inspiral and most of the plunge (which starts at $u/2M \simeq 240$). It is only at the end of the plunge, just before light-ring crossing, (and during ring-down) that one notices a difference (smaller than about 5%) in modulus. To further study the difference in frequency of the two signals, we compare in Fig. 5 the time evolution of the *phases* of the two signals (with the convention $\Psi = e^{-i\phi}$, so that $\dot{\phi} = +\omega$): the *matched* instantaneous gravitational wave phase ϕ_{22}^{EOB} versus the exact one $\phi_{22}^{(\text{exact})}$. These quantities are computed from time integration of the instantaneous frequencies from an initial time t_0 starting with $\phi_0 = 2\varphi_0$ where φ_0 is the initial orbital phase. The visual agreement between the exact phase (black line) and the matched phase (red line) is *so good that the two lines can barely be distinguished*. At a quantitative level, the phase difference $\Delta\phi_{22}^{\text{gw}} \equiv \phi_{22}^{\text{EOB}} - \phi_{22}^{(\text{exact})}$

⁹ In view of this, a useful alternative to the a, b NQC factor in braces used above, is to use instead a factorized complex NQC waveform correction of the form, $(1 + a'p_{r_*}^2/(r\Omega)^2)\exp(+ib'p_{r_*}/(r\Omega))$, in which a' affects only the modulus, and b' only the phase. The (approximate) analytic constraint on the modulus discussed below then becomes simply $2a' = 1$.

¹⁰ If one wanted to have a C^∞ transition between the two waveforms one could replace $\theta(t - t_m)$ by one of Laurent Schwartz’s well-known smoothed step functions (or “partitions of unity”) $\theta_\epsilon((t - t_m)/\delta)$

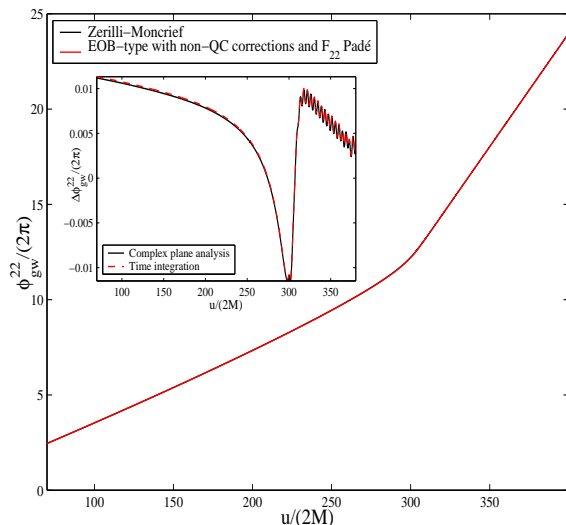


FIG. 5: Analytic and numerical gravitational wave phases versus (shifted) retarded time. As they are very nearly superposed, the inset shows the difference between the two phases (computed, as a check, by means of two independent methods).

is an important diagnostics which is shown in the inset of Fig. 5 (after adding a constant offset). This has been computed by two separate methods. The first one (red dashed line) computes $\Delta\phi_{22}^{gw}$ by straightforward time integration of the difference between $M\omega_{22}^{EOB}$ and $M\omega_{22}$. The second computation (black solid line) does not involve any time integration, it just evaluates the argument of the ratio of the two complex numbers Ψ_{22}^{EOB} and $\Psi_{22}^{(exact)}$:

$$e^{-i\Delta\phi_{22}^{gw}} = \frac{\Psi_{22}^{EOB}}{\Psi_{22}^{(exact)}} \frac{|\Psi_{22}^{(exact)}|}{|\Psi_{22}^{EOB}|}. \quad (20)$$

As shown in the inset of Fig. 5 there is an excellent consistency between the two methods.

Fig. 5 exhibits our most important final result: the maximum phase difference, during the whole transition from inspiral to plunge, between our improved EOB signal and the exact one is of the order of $\pm 1.1\%$ of a cycle. Note that the ripples in the late-time part of $\Delta\phi_{22}^{gw}$ are (obviously) related to the absence of negative frequency modes in the matched waveform.

This excellent analytical description of the exact waveform (phasing to $\pm 1.1\%$ of a cycle, and a rather accurate modulus, see Fig. 3) was obtained by combining the several improvements to the EOB method introduced above, and by using the specific numerical values of the new parameters a_{RR} , a , b , t_m , δ quoted above. Note, however, that there remains some flexibility in the numerical values of these parameters. We leave to future work a detailed discussion of this issue. Let us only note here that the “good choices” of these parameters (minimizing the

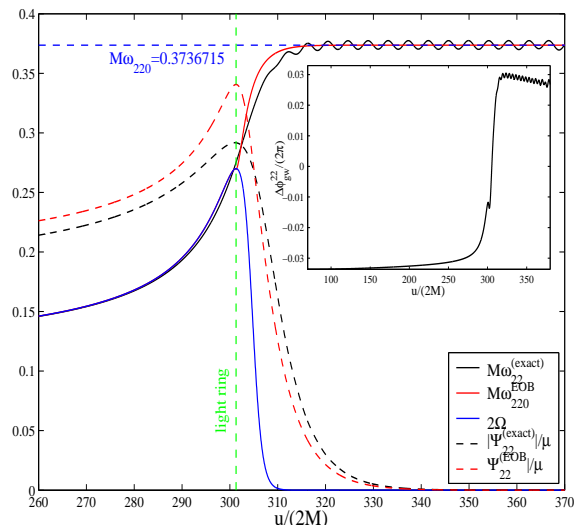


FIG. 6: Comparison between the moduli and the phases of two waveforms: the “exact” numerical one, and a non-optimized analytic one based on a coarser implementation of the EOB philosophy (no PN corrections, no explicit NQC corrections, $N = 3$ QNMs, nearly instantaneous matching at the light ring). See text for details.

maximum (absolute) dephasing¹¹) are correlated, and that the values we have used above are near optimal in the following sense: if, for example, we keep fixed the matching comb parameters t_m and δ , and vary a in the interval $[0.3, 0.8]$, the best possible complementary values of b that we could find (varying in the interval $[0.2, 0.5]$) were found to lead to minimax dephasings larger than 1.1%, but remaining smaller than 3%. We also explored the sensitivity to the choice of the matching comb. For instance, if we keep fixed only the center of the matching interval at $t_m/(2M) = 299.6$, and increase δ/M by a factor 2 (to $\delta/M = 14.4$) and then look for the best possible values of the parameters a and b , we find that the minimax dephasings are increased from 1.1% to about 2%. On the other hand, if (still keeping fixed t_m) we decrease δ/M to 1.8, and then look for the best possible a and b , we find that the minimax dephasings are increased from 1.1% to 2.5%. Similar sensitivities are also reached if we keep fixed δ/M (to the near optimal value 7.2), but move the center of the interval: for example, $t_m/(2M) = 298$ leads to a minimax of 2%, while $t_m/(2M) = 301$ gives 4%, so that we obtain correspondingly less accurate descriptions of the waveform.

On the other hand, as we shall discuss in detail in a separate publication, even much simplified versions of our matching technique can lead to rather impressively good results, notably for the phasing. To quote one particu-

¹¹ We shall refer to the minimum value of the maximum absolute value of the dephasing (over the whole inspiral-plunge-merger period) as the “minimax” dephasing.

larly simple example, the standard quadrupole formula in the quasi-circular approximation (in the sense of Eq. (14) with $F_{22} = 1$, $a = b = 0$ and $N = 5$), still gives a quite tiny dephasing, $\Delta\phi_{22}^{\text{gw}}/(2\pi) \lesssim 2\%$, though the evolution of the modulus is less well reproduced.

Finally, we pedagogically illustrate in Fig. 6, in a “contrasting” manner, the effect of the various improvements introduced above by showing how the waveform comparison of Fig. 3 gets modified when *not* using them, but using instead the type of coarser implementation of the EOB philosophy used in previous work [1, 3, 17, 21, 24]. More precisely, the EOB-type analytical waveform used in Fig. 6 was obtained by: (i) using (as originally proposed in Ref. [1]) the following (Newtonian-order and Kepler-law-assuming) restricted quadrupole waveform

$$\Psi_{22}^{NK}(t) = -4\mu\sqrt{\frac{\pi}{30}}\Omega^{2/3}e^{-2i\varphi}, \quad (21)$$

without any explicit PN (F_{22}) corrections, nor any NQC (a, b) corrections; (ii) only 3 (positive-frequency) QNMs; and, rather crucially, (iii) by matching the plunge and ring-down waveforms in a very small interval ($\delta/M = 0.9$ instead of our preferred 7.2) around the maximum of the orbital frequency. [Indeed, the matching of the two waveforms and their derivatives at a sharply defined moment is equivalent to considering the $\delta \rightarrow 0$ limit of our comb-matching technique]. By contrasting Fig. 6 with the right panel of Fig. 3 we see that: (i) the modulus of the analytical waveform is now distinctly larger than the exact one during the inspiral (because of the lack of PN corrections); (ii) the modulus becomes significantly larger than the exact one at the end of the plunge (because of the use of the Kepler-law-assuming $\propto \Omega^{2/3}$, which, as pointed out in [24] tends to overestimate the amplitude); (iii) the post-matching analytical frequency jumps up from the (doubled) maximum orbital frequency significantly more vertically than before, thereby decoupling too soon from the exact frequency, and accruing a larger dephasing than before (because of the too localized matching, and – to a lesser degree – the use of only 3 QNMs). Note, however that (as exhibited in the inset) this “coarser” EOB-type implementation still succeeds in following the phase of the exact signal to a rather impressive $\pm 3.5\%$ of a cycle.

V. CONCLUSIONS

We have presented a first attack on the problem of computing analytic template waveforms, describing the complete binary black hole coalescence phenomenon (from early inspiral to late ring-down) that are both *effectual* and *faithful* (in the terminology of Ref. [20]). We have restricted our analysis to the small-mass-ratio limit without spin, a problem that is amenable of a semi-numerical investigation based on a synergic use of black

hole perturbation theory and PN-based EOB results [26].

Our analytic approach is based on the Effective One Body (EOB) method [1, 2, 22, 23, 24]. The current implementations [1, 3, 17, 21, 24] of this method have been recently shown [17] to define *effectual* templates for the coalescence of comparable-mass (non-spinning) systems in the full mass range of interest for ground-based GW detectors. Our aim is to *improve* the implementation of the EOB method so as to construct *high-accuracy, faithful* templates. Our strategy towards this aim is to understand, element by element, the physics behind each feature of the waveform, by comparing generalized, multi-parameter EOB-based waveforms to “exact” waveforms obtained by numerical relativity approaches. In this first paper, we have tapped the information contained in small-mass-ratio waveforms, which can rather easily be computed very fast and with high-accuracy.

Our main achievements are: (i) a better description of radiation reaction during the plunge (by taking into account non-quasi-circular effects); (ii) a refined analytical expression for the $(\ell, m) = (2, 2)$ waveform (which includes a resummation of tail effects, a 3PN-accurate “non-linear” amplitude correction, and the inclusion of non-quasi-circular corrections); (iii) an improved technique for matching the plunge and ring-down waveforms (which is based on an improved understanding of the physical elements entering this matching: origin of the excitation of quasi-normal modes, sign of their frequencies, use of an extended matching interval). The implementation of these improvements has led us to the explicit computation of EOB-type analytic waveforms that accurately reproduce (both in its phase and its amplitude) the exact waveform during the whole transition. In particular, the phase difference stays within $\pm 1.1\%$ of a cycle. Such a good result in the small mass-ratio case rises the hope that a comparably good agreement could also be achieved in the comparable-mass case. This will be the object of future work [41].

Acknowledgments

We thank E. Berti and A. Buonanno for assistance during the conception of this work; R. De Pietri and L. Rezzolla for discussions, and A. Tartaglia for support. Part of the numerical work has been carried out by means of the commercial software MATLABTM. The MATLABTM implementation of the *complex* Γ -function in Eq. (16) is due to Paul Godfrey and can be found at: <http://home.att.net/~numericana/answer/info/godfrey.htm>. AN is grateful to IHES and AEI for hospitality during the inception and development of this work; he also thanks K. Kokkotas and ILIAS for financial support.

-
- [1] A. Buonanno and T. Damour, Phys. Rev. D **62**, 064015 (2000).
- [2] A. Buonanno and T. Damour, Phys. Rev. D **59**, 084006 (1999).
- [3] A. Buonanno, Y. Chen and T. Damour, Phys. Rev. D **74**, 104005 (2006).
- [4] R. H. Price and J. Pullin, Phys. Rev. Lett. **72**, 3297 (1994).
- [5] J. G. Baker, B. Brügmann, M. Campanelli, C. O. Lousto and R. Takahashi, Phys. Rev. Lett. **87**, 121103 (2001).
- [6] J. G. Baker, M. Campanelli, C. O. Lousto and R. Takahashi, Phys. Rev. D **65**, 124012 (2002).
- [7] F. Pretorius, Phys. Rev. Lett. **95**, 121101 (2005).
- [8] M. Campanelli, C. O. Lousto, P. Marronetti and Y. Zlochower, Phys. Rev. Lett. **96**, 111101 (2006).
- [9] P. Diener, F. Herrmann, D. Pollney, E. Schnetter, E. Seidel, R. Takahashi, J. Thornburg, J. Ventrella, Phys. Rev. Lett. **96**, 121101 (2006).
- [10] M. Campanelli, C. O. Lousto and Y. Zlochower, Phys. Rev. D **73**, 061501(R) (2006).
- [11] J. G. Baker, J. Centrella, D. I. Choi, M. Koppitz and J. van Meter, Phys. Rev. D **73**, 104002 (2006).
- [12] J. G. Baker, M. Campanelli, F. Pretorius and Y. Zlochower, Class. Quant. Grav. **24**, S25 (2007).
- [13] M. Campanelli, C. O. Lousto and Y. Zlochower, Phys. Rev. D **74**, 041501(R) (2006).
- [14] J. A. Gonzalez, U. Sperhake, B. Brügmann, M. Hannam and S. Husa, Phys. Rev. Lett. **98**, 091101 (2007).
- [15] J. Thornburg, P. Diener, D. Pollney, L. Rezzolla, E. Schnetter, E. Seidel and R. Takahashi, arXiv:gr-qc/0701038 (2007).
- [16] M. Koppitz, D. Pollney, C. Reisswig, L. Rezzolla, J. Thornburg, P. Diener and E. Schnetter, arXiv:gr-qc/0701163 (2007).
- [17] Y. Pan, A. Buonanno, J. G. Baker, J. Centrella, B. J. Kelly, S. T. McWilliams, F. Pretorius and J. R. van Meter, arXiv:0704.1964 [gr-qc], (2007).
- [18] P. Ajith *et al.*, arXiv:0704.3764 [gr-qc], (2007).
- [19] A. Buonanno, Y. Chen and M. Vallisneri, Phys. Rev. D **67**, 024016 (2003) [Erratum-ibid. D **74**, 029903 (2006)].
- [20] T. Damour, B. R. Iyer and B. S. Sathyaprakash, Phys. Rev. D **57**, 885 (1998).
- [21] A. Buonanno, G. B. Cook and F. Pretorius, Phys. Rev. D **75**, 124018 (2007).
- [22] T. Damour, P. Jaranowski and G. Schäfer, Phys. Rev. D **62**, 084011 (2000).
- [23] T. Damour, Phys. Rev. D **64**, 124013 (2001).
- [24] T. Damour and A. Gopakumar, Phys. Rev. D **73**, 124006 (2006).
- [25] T. Damour and A. Nagar, to appear in the Proceedings of the 11th Marcel Grossman Meeting on Recent Development in Theoretical and Experimental General Relativity, Gravitation and Relativistic Field Theories (MG11), arXiv:gr-qc/0612151 (2006).
- [26] A. Nagar, T. Damour and A. Tartaglia, Class. Quant. Grav. **24**, S109 (2007).
- [27] T. Damour, P. Jaranowski and G. Schäfer, Phys. Lett. B **513**, 147 (2001).
- [28] L. Blanchet, T. Damour and G. Esposito-Farese, Phys. Rev. D **69**, 124007 (2004).
- [29] L. Blanchet, B. R. Iyer and B. Joguet, Phys. Rev. D **65**, 064005 (2002) [Erratum-ibid. D **71**, 129903 (2005)].
- [30] L. Blanchet and B. R. Iyer, Phys. Rev. D **71**, 024004 (2005).
- [31] L. Blanchet, T. Damour, G. Esposito-Farese and B. R. Iyer, Phys. Rev. Lett. **93**, 091101 (2004).
- [32] A. Nagar and L. Rezzolla, Class. Quant. Grav. **22**, R167 (2005) [Erratum-ibid. **23**, 4297 (2006)].
- [33] A. Buonanno and T. Damour, in Proceedings of the 9th Marcel Grossmann Meeting on Recent Developments in Theoretical and Experimental General Relativity, Gravitation and Relativistic Field Theories (MG 9), (World Scientific, 2002), Pt. B, pp. 1637-1638; arXiv:gr-qc/0011052.
- [34] S. Chandrasekhar and S. Detweiler, Proc. R. Soc. London A **344**, 441 (1975).
- [35] E. W. Leaver, Proc. R. Soc. London A **402**, 285 (1985).
- [36] T. Damour and A. Nagar, in preparation.
- [37] M. Davis, R. Ruffini, W. H. Press and R. H. Price, Phys. Rev. Lett. **27**, 1466 (1971); M. Davis, R. Ruffini and J. Tiomno, Phys. Rev. D **5**, 2932 (1972).
- [38] K. S. Thorne, Rev. Mod. Phys. **52**, 299 (1980).
- [39] H. Asada and T. Futamase, Phys. Rev. D **56**, R6062 (1997).
- [40] H. Tagoshi and M. Sasaki, Prog. Theor. Phys. **92**, 745 (1994).
- [41] T. Damour, A. Nagar, P. Diener, L. Rezzolla, D. Pollney and R. Takahashi, in preparation.